

Research Paper

# Magnetic ternary nanohybrids for nonviral gene delivery of stem cells and applications on cancer therapy

Rih-Yang Huang\*, Yee-Hsien Lin\*, Ssu-Yu Lin, Yi-Nan Li, Chi-Shiun Chiang and Chien-Wen Chang<sup>✉</sup>

Department of Biomedical Engineering and Environmental Sciences, National Tsing Hua University, Hsinchu 30013, Taiwan R.O.C.

\* R.-Y. Huang and Y.-H Lin contributed equally to this work

✉ Corresponding author: \*Tel.: 886-3-5715131 ext. 35531. Fax: 886-3-5718649. Email: chienwen@mx.nthu.edu.tw.

© Ivyspring International Publisher. This is an open access article distributed under the terms of the Creative Commons Attribution (CC BY-NC) license (<https://creativecommons.org/licenses/by-nc/4.0/>). See <http://ivyspring.com/terms> for full terms and conditions.

Received: 2018.08.18; Accepted: 2019.02.02; Published: 2019.04.13

## Abstract

Cancer toxic agent-expressing mesenchymal stem cells (MSCs), which possess inherent tumor migration and penetration capabilities, have received increasing attention in cancer therapy. To ensure that this approach is successful, safe and efficient gene delivery methods for stem cell engineering must be developed.

**Methods:** In this study, a magnetic ternary nanohybrid (MTN) system comprising biodegradable cationic materials, nucleic acids, and hyaluronic acid-decorated superparamagnetic iron oxide nanoparticles was proposed to construct stem cells expressing the tumor necrosis factor-related apoptosis-inducing ligand (TRAIL) via magnetic force and receptor dual targeting.

**Results:** The CD44/magnetic force-mediated enhanced cellular uptake of MTNs by human mesenchymal cells (hMSCs) was confirmed *in vitro*. Highly efficient transfection was attained using MTNs without having any detrimental effect on the tumor migration and penetration capabilities of hMSCs. TRAIL expressed by the MTN-transfected hMSCs displayed strong anticancer effects through the activation of caspase-3 apoptotic signaling. The MTN-transfected hMSCs can be clearly imaged using magnetic resonance imaging techniques *in vivo*. In an orthotopic xenograft cancer model, MTN-transfected TRAIL-expressing hMSCs significantly suppressed the progression of human glioma (U87MG) and prolonged the survival of the animal.

**Conclusions:** These findings suggest the considerable potential of utilizing MTNs for effectively constructing tumor toxic agent-expressing stem cells for treating malignant cancers.

Key words: Genetically-engineered mesenchymal stem cells, hyaluronic acid, superparamagnetic iron oxide nanoparticles, gene magnetofection, TRAIL glioma therapy

## Introduction

Effective drug delivery deep into tumors remains a major challenge for cancer therapy. High interstitial hypertension and dense extracellular matrix inside a tumor account for poor drug diffusion and penetration [1]. Without proper treatment, the unattended hypoxic cancer cells would certainly increase the risk of tumor recurrence. In the recent decade, stem cells have received increasing attention due to their cancer drug delivery potential [2-5]. Stem cells possess strong tumor tropism, an ability of actively migrating toward tumors. Although the

mechanism is not completely understood yet, chemotaxis is thought to serve a primary role in this process [6, 7]. Cancer cells secrete several soluble factors such as growth factors, chemokines, and cytokines; these factors form a gradient around tumors. The binding of these chemotactic factors to the stem cell surface receptors triggers the assembly of the cytoskeleton for directional cell crawling toward tumors [8, 9]. Various stem cells, including neural stem cells [10, 11], induced pluripotent stem cells [12, 13], and mesenchymal stem cells (MSCs) [14, 15], have

presented excellent tumor migration abilities. Compared with adult stem cells from other rare sources, MSCs are advantageous because they can be isolated from multiple sources and have low immunogenicity. Thus, MSCs may be utilized as a safe and cost-effective drug delivery platform for malignant cancer treatment.

Glioblastoma (GBM) is one of the most devastating human malignant cancers [16-18]. Effective treatments for GBM are lacking primarily due to rapid cancer propagation and highly infiltrative growth into normal brain tissues. As a result, patients who receive conventional treatments (i.e., surgery, chemotherapy, radiation therapy, or a combination of two of more therapies) present a low 5-year survival rate (<5%) [19]. Tumor necrosis factor-related apoptosis-inducing ligand (TRAIL), a type II transmembrane protein, is a potent anticancer ligand against various human cancers. TRAIL binds to the death receptor 4/5 (DR 4/5) overexpressed on cancer cells and triggers the caspase signaling pathway [20]. NK cells and CD8<sup>+</sup> T cells, despite expressing the TRAIL receptors, are resistant to TRAIL-mediated apoptosis inducing effects [21]. Thus, use of TRAIL as a safe and effective option in cancer therapy has attracted considerable attention because of its capability of selective induction of apoptosis in cancer cells and not normal cells. However, the applications of TRAIL are limited due to low *in vivo* protein stability (half-life of human TRAIL in serum is less than 30 min) [22]. Various TRAIL-stabilizing strategies, such as PEGylation [23] and protein immobilization on nanoparticles [24], have presented an ability to increase serum half-life for obtaining superior anticancer efficacy. Alternatively, tumor tropic stem cells can be genetically engineered to become a cell-based “protein factory” for presenting fresh TRAIL to tumors. Thus, viral gene vectors are commonly utilized to construct TRAIL-expressing stem cells that have promising apoptosis-inducing effects on human cancer cells [11, 25]. Despite their efficient gene delivery performance, further clinical translation of viral gene vectors is limited due to high production cost and adverse immune reactions [26]. Nanoparticle-based gene delivery methods, although less efficient, have gained increasing interests due to their advantages in terms of clinical translation, such as scaling up, low immunogenicity, and versatile material designs.

Various cationic polymer- or lipid-based materials have been proposed for stem cell gene delivery, with efficiency ranging from 2% to 35% [27]. To effectively construct genetically engineered stem cells, efficient and nontoxic gene delivery materials

are still highly required. In recent years, incorporation of inorganic nanoparticles has emerged as an effective method to enhance the gene delivery efficiency of cationic carriers [28]. The enhancement can be attributed to the improved colloidal stability and cellular uptake of cationic polymers complexing with inorganic nanoparticles. Incorporation of inorganic metal nanoparticles also confers additional theranostic functions such as the photothermal effect [29-31], imaging contrast [32, 33], and fluorescence imaging [34]. In this study, we proposed a novel magnetic ternary nano hybrid (MTN) system for gene delivery into human MSCs. The nano hybrid can be rapidly fabricated by electrostatically assembling hyaluronic acid (HA)-decorated superparamagnetic iron oxide (SPIO) nanoparticles (HA-SPIOs) with common cationic polyplexes. A ligand exchange reaction was utilized to prepare HA-SPIO. HA is a biocompatible anionic polymer capable of binding to CD44 receptor-overexpressing MSCs [35, 36]. A combination of HA with SPIO is anticipated to facilitate stem cell uptake of cationic nanocomplexes through dual CD44- and magneto-targeting effects. Here, HA-SPIO was first synthesized and characterized to determine its material properties in detail. A series of MTNs were prepared by complexing HA-SPIO with various cationic materials and then were examined for estimating the *in vitro* transfection efficiency. The effects of magnetic and CD44 dual targeting on the transfection efficiency of MTN were investigated *in vitro*. Tumor tropism of MTN-constructed TRAIL-expressing hMSCs (TRAIL-hMSCs) was examined using a transwell model and three-dimensional spheroid model. Finally, using an orthotopic human glioma xenograft model, magnetic resonance imaging (MRI) of the MTN-constructed TRAIL-hMSCs was performed and the therapeutic efficacy of the cells was investigated.

## Experimental Section

### Materials

Branch polyethylenimine (25kDa) was purchased from Sigma-Aldrich (St. Louis, MO, USA). Linear PEI (20kDa) was purchased from PolyScience (Warrington, PA, USA). Paraformaldehyde (PFA) were purchased from Alfa Aesar (Ward Hill, MA, USA).  $\beta$ -cyclodextrin ( $\beta$ -CD), amiloride and chlorpromazine (CPZ) were purchased from TCI (Tokyo, Japan). The gene expression vectors were prepared by cloning TRAIL gene (Costumed synthesis by Genedirectx), mOrange or firefly luciferase reporter gene (pGL3-basic, Promega) into the downstream of CMV promoter of pcDNA3 (Invitrogen) vector. Each pDNA was amplified in

*Escherichia coli* (DH5- $\alpha$ ) and purified using plasmid midiprep kit (Macherey Nagel, Germany). TOTO-3, LB broth and Alexa fluor  $\text{\textcircled{R}}$  594 goat anti-rabbit IgG (H+L) were purchased from Life Technologies (Gaithersburg, MD, USA). Hyaluronic acid (HA) (100 kDa) was purchased from Lifecore Biomedical, Rabbit anti-active caspase-3 antibody and Transwell were purchased from BD. MTT and ampicillin were purchased from MDBio.

### Synthesis and characterizations of HA-SPIO

SPIOs were synthesized using thermal decomposition methods described in our previous work.[37] The HA-SPIO was synthesized by ligand exchange [38] for oleic acid (OA) replacement with HA onto the SPIO surface. 2 mg SPIO were added into 20 mg HA in 1 mL deionized water and 9 mL DMSO. The mixture was sonicated using ultrasonic bath (DC150H, Delta) for 4 hours. The HA-SPIO was collected by magnet and resuspended in 1 mL deionized water. After magnetic collection and washed with deionized water twice, HA-SPIO was resuspended in 1 mL deionized water and filtered through 0.2  $\mu\text{m}$  PVDF syringe filter before further usage. The iron content of HA-SPIO was determined by KSCN method [39]. To obtain the nano-morphology of HA-SPIO, as-synthesized HA-SPIO in deionized water was deposited on the copper grid with support films of formvar/carbon (Ted Pella, Redding, CA) and observed using TEM (JEM-1200EX II, JEOL, Japan). The magnetism and hysteresis loop of OA-SPIO and HA-SPIO at 300 K were examined by Superconducting Quantum Interference Device (Quantum Design MPMS-XL, USA). The particle size and surface potential of each nanocomposite were measured by dynamic light scattering (Zetasizer Nano Series, Malvern, UK).

### Synthesis of preparation of MTN

Poly  $\beta$ -amino ester (PAE) was synthesized referred to previous report [40]. Disulfide-linked PEI (SPEI) was synthesized according to our previous work [37]. The cationic polyplex was first prepared at various nitrogen/phosphate (N/P) ratios as noted in Figure 2. For PEI/pDNA polyplex formation, pDNA (1  $\mu\text{g}$  in 12  $\mu\text{L}$  5% glucose solution) was mixed with branch polyethylenimine (bPEI, 25kDa), SPEI or linear polyethylenimine (LPEI) prepared in 12  $\mu\text{L}$  5% glucose solution and then incubated at room temperature for 20 minutes. For PAE/pDNA polyplex formation, pDNA (1  $\mu\text{g}$  in 50  $\mu\text{L}$  acetate buffer (25 mM, pH 5.2)) was added into PAE polymer in the same volume of acetate buffer and incubated at room temperature for 15 minutes. Lipofectamine/pDNA was prepared according to manufactory protocol. To

prepare the ternary MTN complexes, cationic polyplex or lipoplex containing 1  $\mu\text{g}$  of pDNA was further mixed with 1.3  $\mu\text{g}$  of HA-SPIO in deionized water and incubated at room temperature for 15 minutes. Successful complexation was verified by the formation of  $^{\text{PAE}}\text{MTN}$  complexes (243 nm) from PAE/pDNA polyplex (161 nm) with HA-SPIO (130 nm) (Figure S1). The as-prepared MTN complexes were used for transfection without further purification.

### Cell culture

Human glioma cell line (U87MG) and batches of hMSCs were purchased from FIRDI, Taiwan. hMSCs were cultured in a-MEM (GIBCO) supplemented with 20% FBS (Hyclone) and 1x Penicillin/Streptomycin (Hyclone); U87MG cells were cultured in MEM (GIBCO) supplemented with 10% FBS and 1x P/S; 293T cells were cultured in DMEM (Hyclone) supplemented with 10% FBS and 1x Penicillin/Streptomycin. The luciferase expressed U87MG cells, hMSCs and eGFP expressed 293T cells and hMSCs were constructed by firefly luciferase gene or eGFP gene encoded lentiviral transduction respectively. The virus production and infection was proceeded according to the protocol from National RNAi Core Facility (Institute of Molecular Biology/Genomic Research Center, Academia Sinica, Taiwan).

### Cellular uptake and mechanism examination

hMSCs were seeded in 24-well plates at cell density of  $5 \times 10^4$  cells per well and cultured at 37°C with 5% CO<sub>2</sub> overnight. TOTO-3 fluorescence dye (Invitrogen) was used to label the pDNA before preparation of  $^{\text{PAE}}\text{MTN}$  polyplex as above mentioned. The hMSCs were washed with PBS and transfected using the TOTO3-DNA- $^{\text{PAE}}\text{MTN}$  for 2 hours (external magnetic field was applied at initial 15 minutes' period). Afterward, the cells were washed with PBS twice, fixed by 4% PFA/PBS for 10 minutes and stained using acti-stain 488 phalloidin (Cytoskeleton) and Hoechst 33342 (Invitrogen) for actin and nucleus indication. For CD44 blocking test, the hMSCs were pretreated with HA in serum free medium for 30 minutes before  $^{\text{PAE}}\text{MTN}$  magnetofection. The transgene expression of hMSCs was quantified by luciferase assay at 48 hours after magnetofection. The non-targeted citric-acid coated SPIO (CA-SPIO) was synthesized based on our previous work [41]. Endocytosis mechanism investigation was performed as hMSCs were pretreated with  $\beta$ -cyclodextrin (2.5 mM), amiloride (0.5 mM) or chlorpromazine (5  $\mu\text{g}/\text{mL}$ ) in serum free a-MEM medium for 30 minutes. Afterward the  $^{\text{PAE}}\text{MTN}$  was used to transfect

hMSCs for 2 hours. At 48 hours post magnetofection, the transgene expression of hMSCs was quantified by luciferase assay (Promega).

### Cytotoxicity & Magnetofection

hMSCs were seeded in 24-well at cell density of  $5 \times 10^4$  per well and incubated at 37°C, 5% CO<sub>2</sub> overnight. hMSCs were washed with PBS and the MTN complex contained 1 µg pcDNA3.mOrange or pcDNA3.luciferase were prepared as above mentioned and added into cells in serum free medium. Once adding the MTN into medium, the magnet was placed under the well-plate for 15 minutes. After the magnet was removed, the cells were kept incubated for another 2 hours before PBS washed and replaced with fresh medium. At 48 hours post-transfection, the cell viability was measured by alamar blue assay (Invitrogen); For evaluating the transfection efficiency, the cells were observed by fluorescence microscopy or lysed for luciferase assay (Promega, Madison, WI, USA) and Bicinchoninic acid protein assay (Pierce Chemical Co, Rockford, IL, USA).

### Transwell migration assay

The migratory ability of hMSCs was evaluated using transwell system (8 µm pore size, BD). Fifty thousand U87MG cells were seeded to each well in 24-well plate and incubated at 37°C, 5% CO<sub>2</sub> overnight. The U87MG cells were washed with PBS and replaced with 0.5 mL of MEM medium contained 0.5% FBS. And  $2 \times 10^4$  of hMSCs or <sup>PAEMTN</sup>transfected hMSCs were added to transwell chamber in 0.2 mL of α-MEM medium containing 0.5% FBS. The transwell insert was transferred into the well for cell migration. After 4 hours, the cells attached on the transwell were fixed with 4% PFA/PBS for 10 minutes and the cells inside the transwell were wiped using Q-tip before cell nucleus staining by Hoechst 33342 (2 µg/mL in PBS). The migrated cells were observed by fluorescence microscopy and counted using ImageJ software.

### Tumor penetration assay

The U87MG spheroid was prepared by hanging drop method. Briefly, eight thousand U87MG cells were resuspend in 15 µL MEM medium supplemented with 10% FBS then drop on the bottom surface of cell culture dish lid. The drops were incubated at 37°C, 5% CO<sub>2</sub> for 48 hours to form the spheroid cells mass. The spheroids were transferred into 96-well plate, which was pre-coated with 100 µL of 0.5% agarose in each well to avoid cells adhesion. Ten thousand of <sup>eGFP293T</sup>, <sup>eGFP</sup>hMSCs or <sup>PAEMTN</sup>transfected <sup>mOrange</sup>hMSCs were added into each well and incubated for another 24 hours. The spheroids

were then washed with PBS and fixed in 4% PFA/PBS for 10 minutes at room temperature. The spheroids were embedded into O.C.T. compound and freeze in -80°C overnight before cryosectioning (10 µm/slices; interslices thickness: 50 µm). The cryosectioned slices were then sealed in ProLong® Gold Antifade Reagent with DAPI (Thermo Fisher Scientific) and observed by fluorescence microscopy.

### Evaluation of in vitro antineoplastic effect

The pcDNA3.TRAIL was used for <sup>TRAIL</sup>hMSCs construction by <sup>PAEMTN</sup>magnetofection. The optimal N/P ratio was evaluated using TRAIL ELISA kit (Peprotech). And the optimal transfection condition on hMSCs was used for the following experiments. For evaluating the in vitro killing effect,  $8 \times 10^3$  of <sup>Luc</sup>U87MG cells were mixed with hMSCs or <sup>mOrange</sup>hMSCs or <sup>TRAIL</sup>hMSCs mediated by <sup>PAEMTN</sup> at cell ratio (U87MG : hMSCs) of 1:3 in each well of 24-well plate. After co-incubation for 48 hours, cells were washed twice with PBS and 200 µL of cell lysis buffer (Promega) was added into each well and the cell lysate was centrifuged at 20,000 g for 2 minutes. 150 µL of each cell lysate was mixed with 50 µL of luciferase reaction buffer (Promega) and the intensity of bioluminescence was read by plate reader (infinite M200; Tecan, Austria). The cell viability of <sup>Luc</sup>U87MG cells was calculated compared to a RLU-to-cell number standard curve prepared by different amount of <sup>Luc</sup>U87MG cells. For active caspase-3 detection, U87MG cells were treated with supernatant from <sup>TRAIL</sup>hMSCs, <sup>mOrange</sup>hMSCs or hMSCs for 3 hours. The cells were then fixed with 4% PFA/PBS for 10 minutes and subjected to immunofluorescence staining.

### Evaluation of therapeutic efficacy on glioma in vivo

The animals were handled in accordance to the animal use protocols approved by National Tsing Hua University, Hsinchu, Taiwan. 6 weeks old BALB/cAnN.Cg-Foxn1nu/CrINarl mice were obtained from the National Laboratory Animal Center (Tainan, Taiwan). The mice were maintained under 12-h light-dark cycle at room temperature (25±1°C) and 60±5% humidity. They were provided with a standard diet during all experimentation. The orthotopic glioma model was set up by intracranial injection of human glioma cell line in nude mice.  $1 \times 10^5$  U87MG cells in 2 µL serum free F-12 medium was stereotactically implanted into 2 mm posterior to the bregma and 1 mm to the right of the midline suture at a depth of 2.5 mm with syringe pump at injection rate of 1 µL/min. After the injection, the hole was fixed by bone wax and skin was sutured.  $2 \times 10^5$  hMSCs, <sup>TRAIL</sup>hMSCs or PBS were intracranial injected at the

same position on day 7, day 12, and day 17 after tumor inoculation. The glioma was observed by MRI once a week and the survival curve was recorded and analyzed by log-rank tests. For *in vivo* active caspase-3 expression, the mice were sacrificed at 72 hours after the first treatment. The mice were then perfused with 10 mL PBS from heart and the brain were extracted and embedded into O.C.T. and freeze in  $-80^{\circ}\text{C}$  overnight. The brain was cryosectioned and subjected to active caspase-3 immunofluorescence staining.

### Magnetic resonance imaging

T2 weighted images of HA-SPIO were obtained by 7T magnetic resonance imaging system (Bruker biospec 70/30 MRI, USA). Aqueous solution of HA-SPIO at different Fe concentrations was prepared and sealed in 250  $\mu\text{L}$  PCR tube. The spin-spin relaxation times ( $T_2$ ) was measured by a multislice multiecho T2 map pulse sequence [42]. The parameters used for scanning were described as follow: static repetition time (TR: 6000 ms) and 32 echo times in 11 ms intervals (TE at 11 ms, 22 ms, 33 ms...), FOV = 6  $\times$  6 mm, matrix size: 256  $\times$  256, NEX = 3. For *in vivo* T2 weighted MR imaging, RARE sequence [43] was chosen for axial brain section images. The glioma-bearing nude mice were anesthetized by 4% isoflurane and scanned. The parameters were set up as follow: TR= 3500 ms/TE= 36 ms, FOV = 3.5  $\times$  3.5 mm, matrix size = 256  $\times$  256, slice thickness = 1 mm; 15 slices; interslice distance = 1 mm; NEX = 3.

### Statistics

Results are presented as the mean and standard error of at least three independent measurements. Two-way ANOVA with Tukey's multiple comparisons test or Student's t-test (unpaired two-tailed) were used for all statistical evaluations.  $p$ -value of less than 0.05 was considered significant ( $p < 0.05$ , \* ;  $p < 0.01$ , \*\* ;  $p < 0.001$ , \*\*\*).

## Results and Discussion

### Synthesis and characterization of HA-SPIO

An MTN system, a ternary nanohybrid system (Figure 1A) consisting of HA-SPIO, cationic materials, and DNA, was used for CD44/magnetic force-mediated gene delivery into human stem cells. Hydrophobic oleic acid (OA)-SPIO (~12 nm) was synthesized using a thermal decomposition process. OA-SPIO and HA dispersed in dimethyl sulfoxide were sonicated in water bath sonicator for 4 hours to generate hydrophilic HA-SPIO. The particle size and surface potential of HA-SPIO were estimated using dynamic light scattering (Figure S1) and were 130 nm and  $-32$  mV, respectively. Formation of SPIO cluster

structures in the nanocomplex was confirmed using transmission electron microscopy (Figure 1B). Standard hysteresis loops of superparamagnetic materials were observed for both HA-SPIO and OA-SPIO by using the superconducting quantum interference device (Figure 1C). The magnetism of HA-SPIO and OA-SPIO was estimated to be 32 and 48 emu/g, respectively. The lower magnetism of HA-SPIO was due to additional weight contribution because of HA modification. Without an external magnetic field, HA-SPIO was highly dispersed in an aqueous solution. The ferrofluidic behavior of HA-SPIO in aqueous was clearly observed under an external magnetic field (Figure 1D). In this study, a straightforward sonication-facilitated polymer exchange step was successfully used to prepare HA-SPIO through the ligand exchange process.

### Magnetofection and cellular uptake mechanism

A series of MTNs were prepared by assembling HA-SPIO with various polyplexes or lipoplexes, including Poly  $\beta$ -amino ester (PAE), linear polyethyleneimine (LPEI), branched polyethyleneimine (bPEI), disulfide-linked polyethyleneimine (SPEI), and lipofectamine. *In vitro* transfection efficiencies of these MTNs were compared by examining their capabilities of delivering the firefly luciferase gene into hMSCs. In a serum-free condition, the transfection efficiencies of the MTNs could be arranged in the following order: PAE > bPEI ~ lipofectamine > LPEI ~ SPEI. The transfection efficiencies of all MTNs were significantly enhanced (e.g., 16 times for PAE-containing MTN ( $^{\text{PAE}}\text{MTN}$ )) when an external magnetic field was applied (Figure 2A). The cell viabilities of the MTNs could be listed in the following order: PAE ~ SPEI > lipofectamine > LPEI > bPEI (Figure 2B). *In vitro* transfection efficiency of the  $^{\text{PAE}}\text{MTN}$  on hMSCs was further evaluated using FACS analysis. The transfection efficiency by MTN were increased from 20% to 65% under a magnetic attraction (Figure S2). Robust magnetofection by  $^{\text{PAE}}\text{MTN}$  was verified by observing similar performance in hMSCs isolated from a different donor source (Figure S3). As the  $^{\text{PAE}}\text{MTN}$  showed the greatest transfection efficiency and negligible cytotoxicity, it was utilized for further construction of TRAIL-expressing hMSCs. Particle size and surface potential of the  $^{\text{PAE}}\text{MTN}$  were 243 nm and 26 mV respectively (Figure S1). The as-prepared MTN complexes were used for transfection without further purification. It was previously proposed that magnetofection can be primarily attributed to magnetically accelerated precipitation on the cell surface. This might be especially valid for cationic gene carriers containing only secondary or tertiary

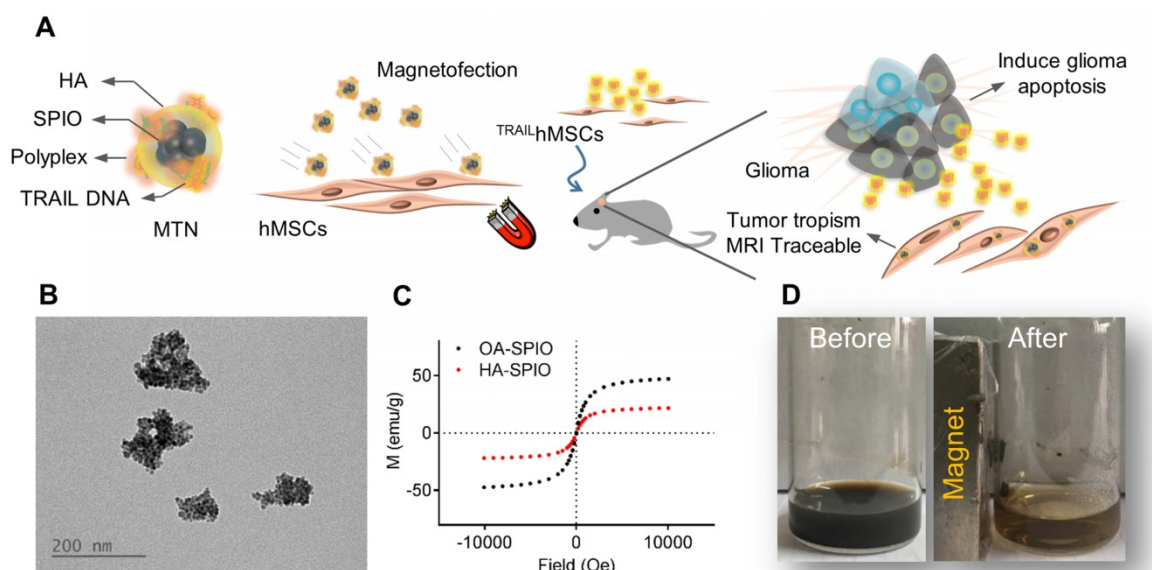


**Figure 1.** Physicochemical characterization of magnetic ternary nanohybrids. (A) Illustration of MTN formation and its applications on glioma treatment. (B) Nanomorphology of HA-SPIO visualized by TEM. (C) The magnetization curve of OA-SPIO and HA-SPIO at 300K. (D) The ferrofluids behavior of HA-SPIO were imaged before and after magnetic attraction.

amines. Tertiary amines (and very few secondary amines) on PAE can only be protonated under an acidic condition (pH 5.2) for complexation with DNA through electrostatic interactions. When transfected in a regular cell culture medium (pH of approximately 7.4), the PAE/DNA polyplexes began to disassemble and aggregate (Figure S4); this could eventually decrease the transfection efficiency. Applying an external magnetic field may accelerate the contact between  $^{PAE}MTN$  and CD44 receptors for subsequent cellular entry. The essential role of HA-CD44 binding on the transfection performance of  $^{PAE}MTN$  was further verified through a HA competition test.

The results revealed (Figure 3A) that the transfection efficiency of  $^{PAE}MTN$  was inversely proportional to the amount of free HA added, thus suggesting the crucial role of HA-CD44 binding on  $^{PAE}MTN$  transfection. The assumption was further strengthened due to a decrease in the transfection efficiency of  $^{PAE}MTN$  in which HA-SPIO was replaced by citric acid (CA)-SPIO (Figure 3B). The transfection efficiencies of these nanoparticles could be listed in the following order: HA-SPIO/PAE/DNA > PAE/DNA complex > CA-SPIO/PAE/DNA. The order reveals the crucial roles of both HA-CD44 binding and magnetic attraction. To investigate the cellular uptake mechanism, various endocytosis inhibitors were tested for their effects on the transfection efficiency of  $^{PAE}MTN$ . Pretreatment with an amiloride or  $\beta$ -cyclodextrin inhibitor significantly decreased the transfection efficiency (Figure 3C), thus implying that caveolea-mediated endocytosis and macropinocytosis [44] were the major cell

internalization pathways for  $^{PAE}MTN$ . Interestingly, the transfection efficiency of  $^{PAE}MTN$  was unexpectedly enhanced by adding chlorpromazine, a clathrin-mediated endocytosis inhibitor. Blocking the clathrin-mediated endocytosis pathway might increase the probability of transporting  $^{PAE}MTN$  through caveolea-mediated endocytosis and macropinocytosis pathways [45, 46] and leads to enhanced transfection efficiency. Enhancement of cell internalization of  $^{PAE}MTN$  due to the magnetic field was also visualized using TOTO3-labeled DNA. The results (Figure 3D) revealed a superior DNA internalization of  $^{PAE}MTN$  in hMSCs with the application of an external magnetic field. In general, the internalized nanoparticles are transported by vesicles undergoing different stages from early endosome, late endosome to lysosome. Effective escape of gene carriers from endosomal/lysosomal compartment is a prerequisite for the subsequent transgene expression. To study the intracellular trafficking, we prepared a fluorescent HA-SPIO by labeling HA with a FITC. Successful preparation of FITC-HA-SPIO was confirmed by detecting the fluorescent spectrum (Figure S5A). Intracellular localization of the FITC-MTN relative to endosome/lysosome was imaged using a confocal microscopy. The results (Figure S5B) show that most of the FITC-MTN were still trapped inside endosome/lysosome after 4 hours of internalization. However, after 24 hours, significant portion of FITC-MTN could be found in the cytoplasm suggesting their successful endosomal escape.

### In vitro antineoplastic effect and tropism behavior of hMSCs

<sup>PAE</sup>MTN gene delivery was utilized to construct TRAIL<sup>hMSCs</sup>. The expression level of human TRAIL was quantified using a human TRAIL enzyme-linked immunosorbent assay. The TRAIL expression level can be presented as follows: <sup>PAE</sup>MTN (with a magnetic field) > <sup>PAE</sup>MTN (without a magnetic field) > PAE > negative control (Figure 4A). TRAIL mRNA expression was quantitated using real-time PCR. Significant elevation (4-fold increase) of TRAIL mRNA was observed by applying an external

magnetic field (Figure S6). Time course expression of TRAIL protein from the transfected hMSCs were analyzed using ELISA assay. Peak expression of TRAIL was observed 48 hours after transfection then decreased thereafter (Figure S7A). The transient expression of TRAIL may be attributed to the loss of plasmids during cell division or inactivation of CMV promoter of the plasmid. Comparing to the un-transfected hMSCs, proliferation rate of the transfected hMSCs was initially slightly reduced on day 2 but recovered after day 5 (Figure S7B).

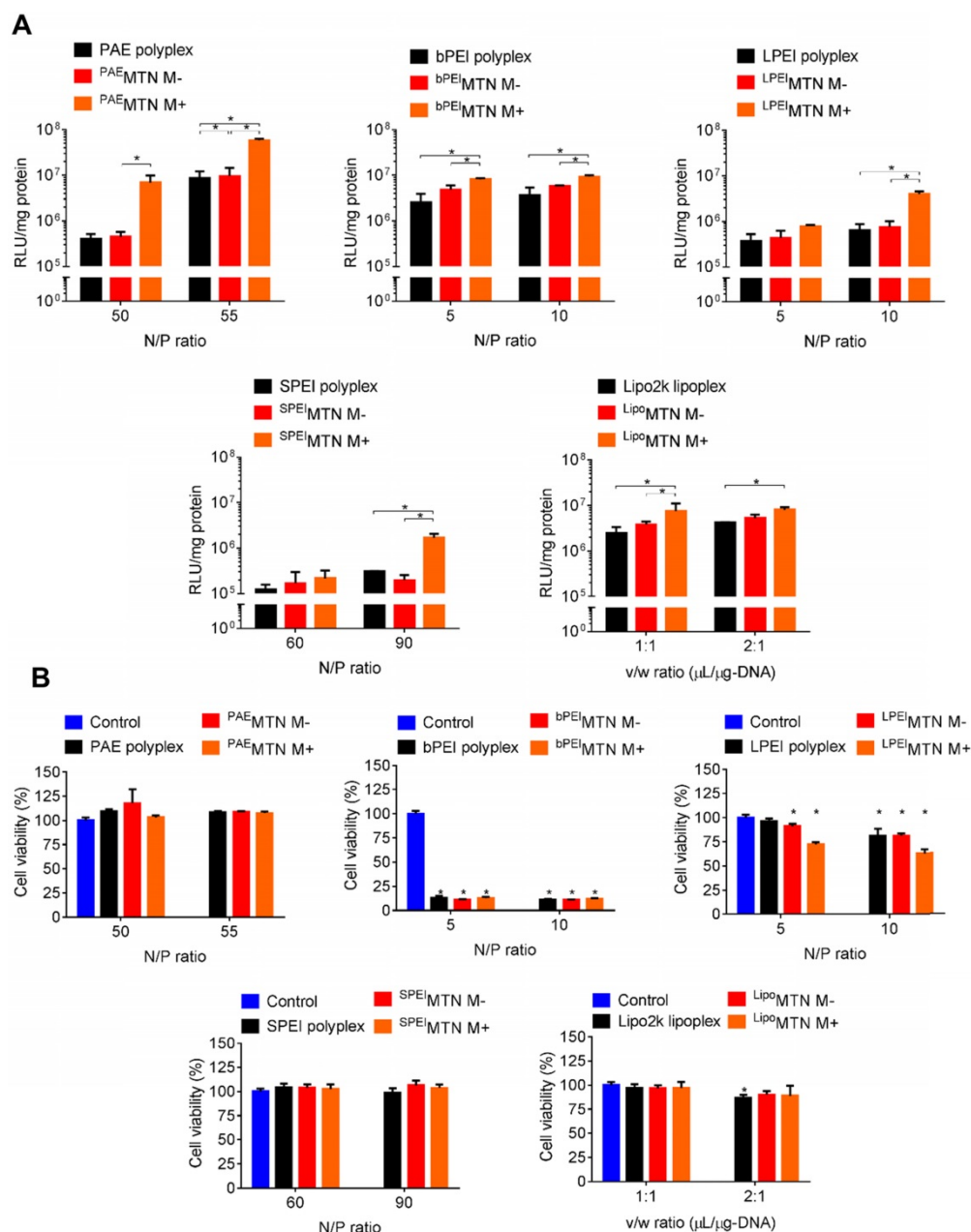


**Figure 2.** In vitro MTN magnetofection on hMSCs and cytotoxicity. (A) The transgene expression and (B) cytotoxicity mediated by HA-SPIO incorporated with different polyplex or lipoplex were analyzed by luciferase assay and alamar blue assay, respectively. Data are mean±s.e.m. and were measured from three independent experiments. \*P<0.01 by two-way ANOVA with Tukey's multiple comparisons test. The definition of abbreviations is concluded as followed. M-: without magnetic attraction. M+: with magnetic attraction. Nitrogen to Phosphate (N/P) ratio: the ratio of the amount of nitrogen in PAE or PEI to the amount of phosphate in pDNA. Volume to weight (v/w) ratio: the ratio of volume (μL) of commercial lipofectamine to the weight (μg) of pDNA.

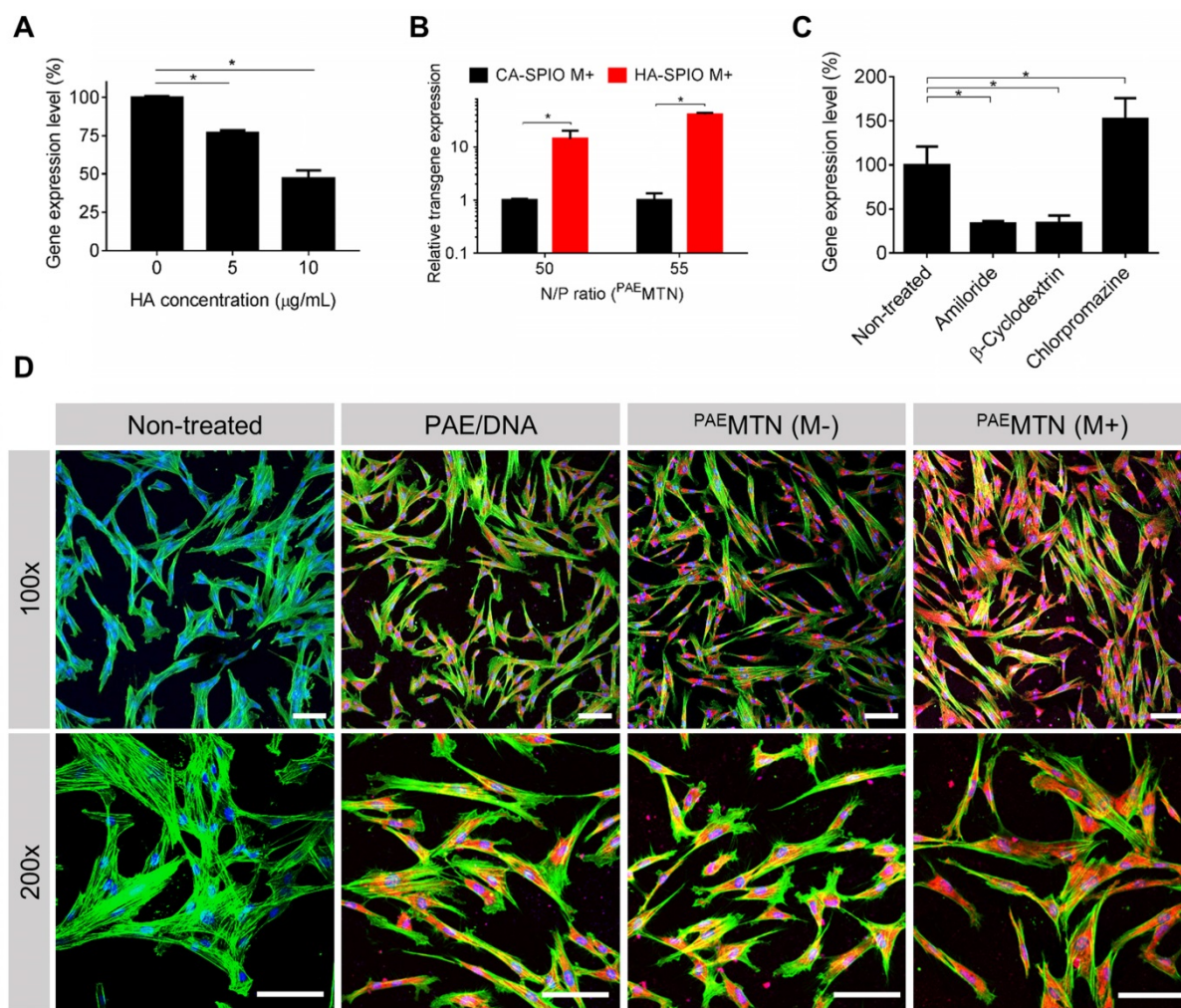


**Figure 3.** Analysis of cellular uptake mechanism. The effect of dual CD44-receptor mediated endocytosis and magnetic-assistance cellular internalization were investigated. The transgene expression level of hMSCs (A) pre-treated HA or (B) transfected with  $^{PAEMTN}$  constructed by non-CD44 targeted CA-SPIO was quantitative analyzed. (C) Different endocytosis inhibitors were used to investigate the uptake mechanism of  $^{PAEMTN}$ . The effect of magnetic-assistance improving the cell internalization of  $^{PAEMTN}$  was evaluated using TOTO3 labeled pDNA. (D) The cell fluorescence images were visualized by confocal laser scanning microscopy (LSM 510, Zeiss). The red fluorescence represented the cell internalized pDNA. Nucleus and cytoskeleton were stained with Hoechst 33342 and Acti-stain 488 phalloidin, respectively. Scale bar in (D): 100  $\mu$ m. Data are mean  $\pm$  s.e.m. Data in (A), (B) and (C) were measured from three independent experiments. \* $P < 0.01$  by student's t-test.

$^{TRAIL}hMSCs$  significantly induced cytotoxic effects on the human glioma cells (U87MG), whereas the unmodified hMSC or PBS treatment did not present any effect on the U87MG cells (Figure 4B). Immunohistological staining of active caspase-3 further confirmed that the observed cell death was mediated by apoptosis (Figure 4C). The results of the image quantification analysis revealed that more than 20% caspase-3-positive cells were induced by TRAIL (Figure 4D). In addition to its anticancer efficacy, it was crucial to verify whether the  $^{PAEMTN}$ -transfected hMSCs still maintained tumor tropism and penetration capability. Thus, the migratory ability of hMSCs after  $^{PAEMTN}$  magnetofection was first evaluated using a transwell model. The migration of  $^{PAEMTN}$ -transfected hMSCs was comparable with that of the untransfected hMSCs (Figure 5A). The tumor penetration capability of the  $^{PAEMTN}$ -transfected hMSCs was further investigated using a

three-dimensional tumor spheroid model. The hanging drop method was used to promote cell-cell interaction to form U87MG tumor spheroids in a serum-containing medium.  $^{PAEMTN}$ -transfected hMSCs ( $^{mOrange}hMSCs$ ), untransfected hMSCs ( $^{eGFP}hMSCs$ ), or  $^{eGFP}HEK293T$  were co-cultured with the U87MG tumor spheroids. After incubating for 24 h, cryosections were prepared from the top to the center of the spheroids for subsequent fluorescence microscopic examinations. The results (Figure 5B) revealed that the  $^{PAEMTN}$ -transfected hMSCs ( $^{mOrange}hMSCs$ ) exhibited a penetration capability similar to that of the non-transfected  $^{eGFP}hMSCs$  in glioma spheroids. By contrast,  $^{eGFP}HEK293T$  cells were used as the negative control and were present on the surface of the spheroids [5]. In summary, these results demonstrated that  $^{PAEMTN}$  magnetofection did not have any detrimental effect on the tumor tropism or penetration capability of hMSCs.

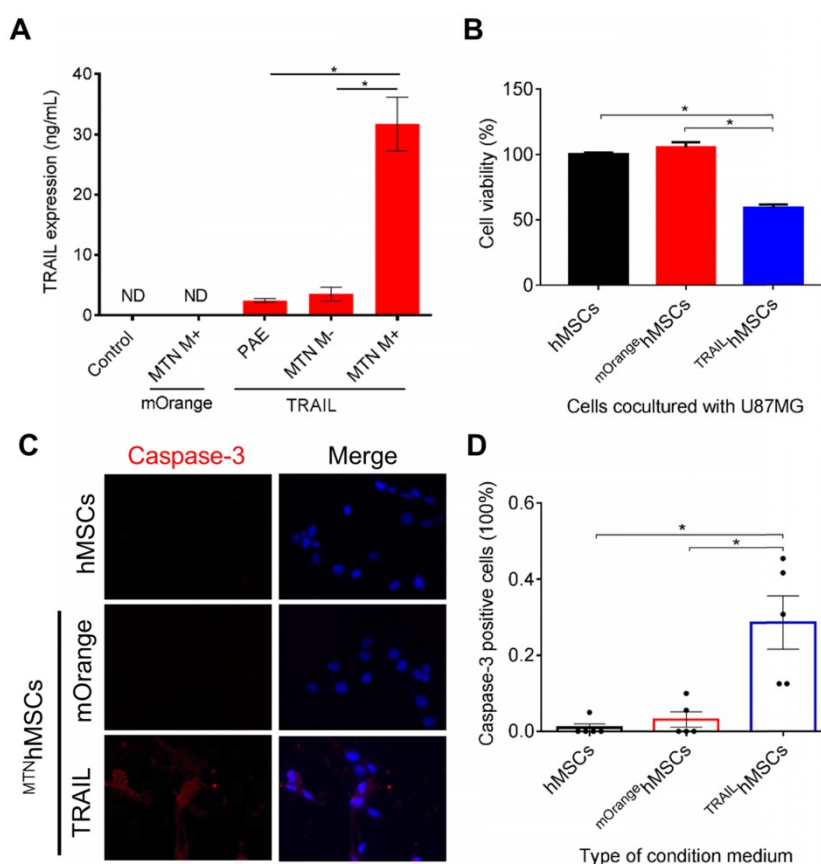


**Figure 4.** Characterization of TRAILhMSCs and in vitro anti-cancer effect against glioma. The amount of TRAIL from TRAILhMSCs and its antineoplastic effect in vitro were examined by (A) ELISA assay and (B) co-culture test respectively. (C) The intracellular active caspase-3 expression of U87MG was stained by caspase-3 immunofluorescence staining. (D) The percentage of active caspase-3 positive cells were calculated by ImageJ. Data in (D) were measured from five independent experiments. In A, \*P<0.01 by student's t-test. In (B) and (D), \*P<0.01 by two-way ANOVA with Tukey's multiple comparisons test.

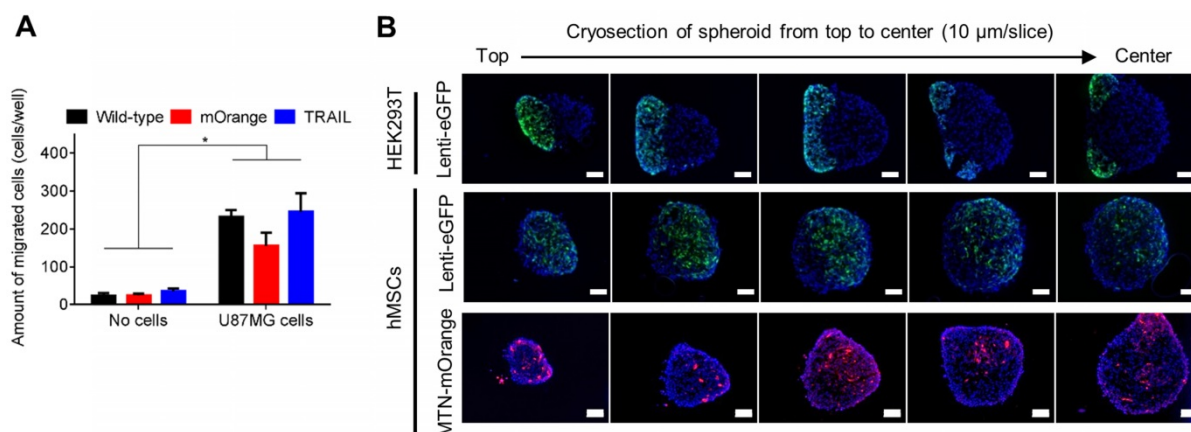


**Figure 5.** Evaluation of hMSCs tumor migration and penetration ability on human glioma cells. (A) The transwell system was used to evaluate the tumor tropism ability of hMSCs. For investigating penetrating ability of hMSCs, eGFP293T, eGFP hMSCs or MTN/mOrange hMSCs were incubated with U87MG spheroids for 24 hours before cryosectioning. (B) Serial cryosectioning images from top to the bottom of spheroid and the cell nucleus on these sections were stained with Hoechst 33342. Green fluorescent eGFP293T or eGFP hMSCs or red fluorescent MTN/mOrange hMSCs were observed using a fluorescence microscopy. Scale bar in (B): 100 μm. Data are mean±s.e.m. Data in (A) were measured from three independent experiments. In (A), \*P<0.01 by two-way ANOVA with Tukey's multiple comparisons test.

### In vitro and in vivo imaging of MTNhMSCs

SPIO, a primary component in the MTN system, is a biocompatible inorganic nanoparticle approved by the Food and Drug Administration for use in MRI [47]. After injections, the *in vivo* distribution of the PAEMTN-transfected hMSCs might be noninvasively tracked using MRI techniques. HA-SPIO exhibited

significant T2 contrast enhancement in the aqueous solution (Figure 6A). The T2 relaxivity of HA-SPIO was 301.2 s<sup>-1</sup> mM<sup>-1</sup> when measured using a 7-T MRI system (Figure 6B), which is higher than that of the commercial MRI contrast agents such as Resovist (141 s<sup>-1</sup> mM<sup>-1</sup>). *In vivo* T2-weighted images of the coronal sections of brain tumor were captured before or after

intracranial injections of the <sup>PAE</sup>MTN-transfected hMSCs. The location of the <sup>PAE</sup>MTN-transfected hMSCs was clearly captured as dark spots on the T2-weighted MR images (Figure 6C). The injected <sup>PAE</sup>MTN-transfected hMSCs presented a value of  $-48.90\% \pm 13.72\%$  on the T2-weighted contrast compared to the surrounding tissues when quantitative imaging analysis was used. In our study, to verify the success of cell injection, MRI was used to verify the initial location of the injected <sup>MTN</sup>hMSCs. In principle, MRI could be further used to track long-term distribution of the injected cells. However, without knowing the survival of injected cells, the acquired images may be complicated by MR signals from both the live and dead <sup>MTN</sup>hMSCs. With this concern in mind, IVIS was utilized to monitor the *in vivo* fate of injected viable luciferase-stem cells (Figure S8). Strong luciferase signal from the injected stem cells was detected 48 hours after injection (Figure S9). No luciferase signal was detected after 1 week indicating the extinction of viable injected stem cells from brain tissues. The short survival of injected hMSCs was also reported by others [48]. In addition, it has been previously confirmed that the intracranially-injected hMSCs did not differentiate during their short survival in brain tissues [49]. We believe these observations has provided a safety basis for using hMSCs as a cell-based drug delivery platform for malignant brain disease treatment.

### **In vivo anti-cancer effect**

GBM is one of the most devastating tumors. Clinical importance of glioma is underscored by its high recurrence rate [50]. Conventional treatments for GBM include surgery, radiation therapy, and chemotherapy. The highly diffusive growth of GBM cells into normal brain tissues has largely limited the efficacy of conventional treatments. Moreover, rapid recurrence due to the induction of drug-resistant cancer cells [51] and tumor bed effects [52] are often observed after radiation therapy or chemotherapy.

Advanced therapeutic strategies such as sustained drug release by using GLIADEL® have been approved as a co-treatment after surgical resection with only moderate improvement [53]. Therefore, development of novel therapeutic strategies for glioma is still highly demanded. hMSCs are capable of actively migrating toward tumors *in vivo*; thus, stem cells have considerable potential of being utilized as drug delivery carriers. However, the systemic injected stem cells may encounter difficulties on entering brain tissues due to the blood brain barrier (BBB) and accumulate in the major organs such as lung, liver and spleen but not brain [54, 55]. Therefore, the intracranial injection, being safe and effective, is considered as a preferred administration route for stem cells-based glioma therapy. In this study, we developed an MTN system as a nontoxic and effective gene delivery tool for constructing <sup>TRAIL</sup>hMSCs. In *in vitro* studies, the <sup>TRAIL</sup>hMSCs revealed promising anti-glioma efficacy without affecting their tumor tropism. To evaluate the *in vivo* antineoplastic effects of <sup>TRAIL</sup>hMSCs, an orthotopic human glioma xenograft model was first developed through intracranial implantation of U87MG cells in nude mice. PBS, hMSCs, or <sup>TRAIL</sup>hMSCs were injected intracranially by using a syringe pump 7 days after U87MG inoculation (Figure 7A). A 7-T MRI was used to noninvasively monitor glioma propagation in the nude mice. Thirty-five days after glioma inoculation, tumor size in the mice that received <sup>TRAIL</sup>hMSCs injections was smaller than that in the mice that received PBS or unmodified hMSCs injections (Figure 7B, 7C). The median survival duration of mice that received PBS or hMSC treatments were 38 and 39 days, respectively (Figure 7D). Significant prolonged survival (46 days) was observed in the mice that received <sup>TRAIL</sup>hMSCs (21.53% increase compared with the control groups). Immunofluorescence staining of glioma sections (Figure 7E) presented significantly active caspase-3 activity after <sup>TRAIL</sup>hMSC treatment. The results clearly demonstrated the antineoplastic potentials of

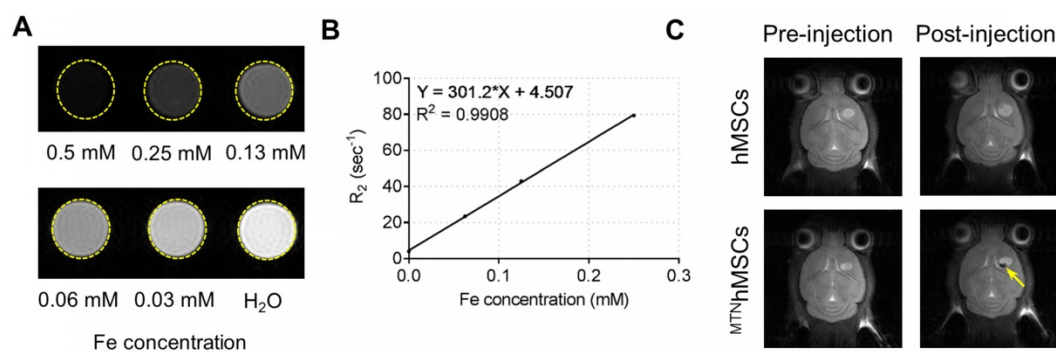


**Figure 6.** MR imaging of HA-SPIO and <sup>TRAIL</sup>hMSCs on U87MG xenograft model. (A) T2-weighted images and (B) T2 relaxivity of HA-SPIO in aqueous solution was examined by 7T MRI. (C) *In vivo* MR images were acquired 24 hours after intracranial injection of hMSCs or <sup>TRAIL</sup>hMSCs. The signal intensity in the region of interest (R.O.I.) was measured using ImageJ.

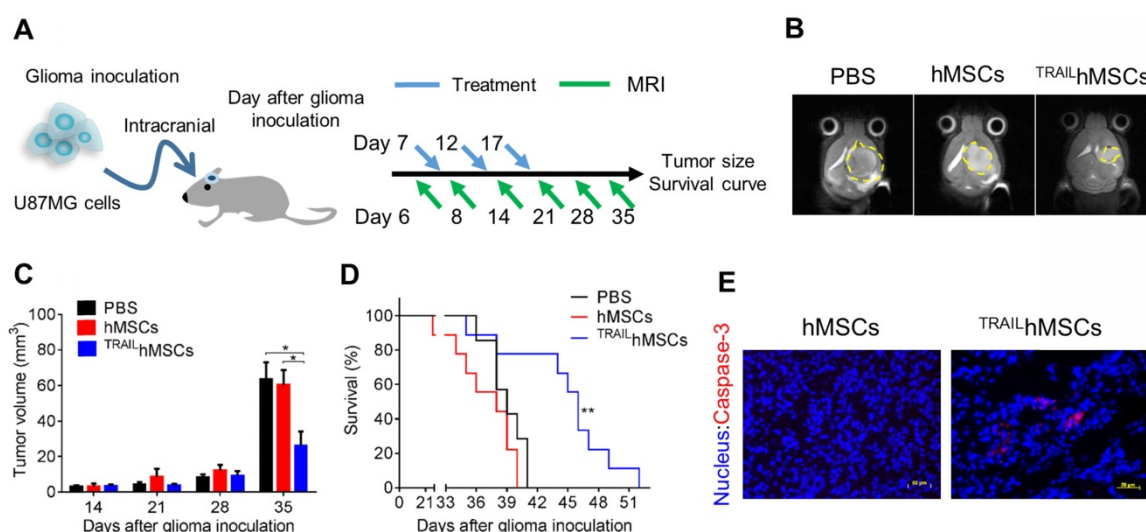


**Figure 7.** *In vivo* anti-cancer effects of TRAIL-hMSCs on orthotopic glioma-bearing xenograft animal model. (A) Scheme of therapeutic plan for orthotopic glioma treatment. (B) *In vivo* T2-weighted MR imaging of brain coronal sections on glioma-bearing mice at 35 days after the glioma inoculation. (C) The tumor volume evolution in glioma-bearing mice, \* $P < 0.05$  by two-way ANOVA with Tukey's multiple comparisons test and (D) survival curve,  $n = 7$  for PBS group and  $n = 9$  for both hMSCs and TRAIL-hMSCs group. \*\* $P < 0.01$  by exact log-rank test. (E) Immunofluorescence staining of active caspase-3 on the brain tumor sections from mice received hMSCs or TRAIL-hMSCs treatments, Scale bar: 50  $\mu\text{m}$ .

MTN-transfected TRAIL-hMSCs against glioma *in vivo*. Regarding the glioma cells acquired resistance to TRAIL, therapeutic efficacy of the TRAIL-hMSCs might be further enhanced by combing with small molecular inhibitors or chemotherapeutic agent [56, 57].

## Conclusion

We successfully constructed an MTN system as an effective nanomaterial-based gene delivery platform for hMSCs. By taking advantage of magnetic attraction and CD44 receptor-mediated endocytosis, the MTN system could effectively deliver genes into hMSCs while maintaining tumor tropism. After local delivery, the MTN-transfected hMSCs could be clearly imaged using MRI techniques. Furthermore, the MTN-constructed TRAIL-hMSCs exhibited conspicuous therapeutic effects in an orthotopic human glioma xenograft model. These findings suggest that the MTN system is an effective nonviral approach to construct tumor toxic agent-expressing stem cells for glioma therapy. In the future, the MTN system might be explored to deliver genes encoding other therapeutic proteins and morphogenic factors for application in cancer therapy and directing stem cell differentiation, respectively.

## Supplementary Material

Supplementary methods and figures.  
<http://www.thno.org/v09p2411s1.pdf>

## Acknowledgments

This research was financially supported by National Health Research Institutes of Taiwan (NHRI-EX105-10221EC), Ministry of Science and

Technology of Taiwan (MOST 107-2113- M-007-028 -) and National Tsing Hua University (107Q2519E1). We thank to Ms. C.-Y. Chien of Ministry of Science and Technology (National Taiwan University) for the assistance in TEM experiments and to 7T animal MRI Core Lab of the Neurobiology and Cognitive Science Center, National Taiwan University for technical and facility supports. The magnetization was measured by using SQUID magnetometer (MPMS XL-7) at the National Chiao Tung University.

## Author Contributions

R.Y. Huang and Y.H. Lin contribute equally to experiment design, data acquisition and analysis and manuscript drafting. S.Y. Lin and Y.N. Li contribute to experiment design and data acquisition. C.S. Chiang contributes to cancer model and interpretation of data. C.W. Chang contributes to study conception and design, interpretation of data and critical revision of the manuscript.

## Competing Interests

The authors have declared that no competing interest exists.

## References

- Jain RK, Stylianopoulos T. Delivering nanomedicine to solid tumors. *Nat Rev Clin Oncol.* 2010; 7: 653-64.
- Huang WC, Lu IL, Chiang WH, Lin YW, Tsai YC, Chen HH, et al. Tumortropic adipose-derived stem cells carrying smart nanotherapeutics for targeted delivery and dual-modality therapy of orthotopic glioblastoma. *J Control Release.* 2017; 254: 119-30.
- Pinho S, Macedo MH, Rebelo C, Sarmiento B, Ferreira L. Stem cells as vehicles and targets of nanoparticles. *Drug Discov Today.* 2018; 23: 1071-78.
- Jiang XY, Wang C, Fitch S, Yang F. Targeting tumor hypoxia using nanoparticle-engineered CXCR4-overexpressing adipose-derived stem cells. *Theranostics.* 2018; 8: 1350-60.

5. Zhang TY, Huang B, Wu HB, Wu JH, Li LM, Li YX, et al. Synergistic effects of co-administration of suicide gene expressing mesenchymal stem cells and prodrug-encapsulated liposome on aggressive lung melanoma metastases in mice. *J Control Release*. 2015; 209: 260-71.
6. Shi Y, Du L, Lin L, Wang Y. Tumour-associated mesenchymal stem/stromal cells: emerging therapeutic targets. *Nat Rev Drug Discov*. 2017; 16: 35-52.
7. Nitzsche F, Muller C, Lukomska B, Jolkkonen J, Deten A, Boltze J. Concise review: MSC adhesion cascade-insights into homing and transendothelial migration. *Stem Cells*. 2017; 35: 1446-60.
8. Spaeth E, Klopp A, Dembinski J, Andreeff M, Marini F. Inflammation and tumor microenvironments: defining the migratory itinerary of mesenchymal stem cells. *Gene Ther*. 2008; 15: 730-38.
9. Wei X, Yang X, Han ZP, Qu FF, Shao L, Shi YF. Mesenchymal stem cells: a new trend for cell therapy. *Acta Pharmacol Sin*. 2013; 34: 747-54.
10. Portnow J, Synold TW, Badie B, Tirughana R, Lacey SF, D'Apuzzo M, et al. Neural stem cell-based anti-cancer gene therapy: a first-in-human study in recurrent high grade glioma patients. *Clin Cancer Res*. 2016; 23: 2951-60.
11. Bago JR, Alfonso-Pecchio A, Okolie O, Dumitru R, Rinckenbaugh A, Baldwin AS, et al. Therapeutically engineered induced neural stem cells are tumour-homing and inhibit progression of glioblastoma. *Nat Commun*. 2016; 7: 10593.
12. Yang M, Liu YL, Hou WX, Zhi X, Zhang CL, Jiang XQ, et al. Mitomycin C-treated human-induced pluripotent stem cells as a safe delivery system of gold nanorods for targeted photothermal therapy of gastric cancer. *Nanoscale*. 2017; 9: 334-40.
13. Liu Y, Yang M, Zhang J, Zhi X, Li C, Zhang C, et al. Human induced pluripotent stem cells for tumor targeted delivery of gold nanorods and enhanced photothermal therapy. *ACS Nano*. 2016; 10: 2375-85.
14. Cao M, Mao J, Duan X, Lu L, Zhang F, Lin B, et al. In vivo tracking of the tropism of mesenchymal stem cells to malignant gliomas using reporter gene-based MR imaging. *Int J Cancer*. 2018; 142: 1033-46.
15. Wu SQ, Yang CX, Yan XP. A dual-functional persistently luminescent nanocomposite enables engineering of mesenchymal stem cells for homing and gene therapy of glioblastoma. *Adv Funct Mater*. 2017; 27: 1604992.
16. Anjum K, Shaguffa BI, Abbas SQ, Patel S, Khan I, Shah SAA, et al. Current status and future therapeutic perspectives of glioblastoma multiforme (GBM) therapy: a review. *Biomed Pharmacother*. 2018; 101: 681-89.
17. Rajesh Y, Pal I, Banik P, Chakraborty S, Borkar SA, Dey G, et al. Insights into molecular therapy of glioma: current challenges and next generation blueprint. *Acta Pharmacol Sin*. 2017; 38: 591-13.
18. Louis DN, Perry A, Reifenberger G, von Deimling A, Figarella-Branger D, Cavenee WK, et al. The 2016 world health organization classification of tumors of the central nervous system: a summary. *Acta Neuropathol*. 2016; 131: 803-20.
19. Omuro A, DeAngelis LM. Glioblastoma and other malignant gliomas: a clinical review. *JAMA*. 2013; 310: 1842-50.
20. Stuckey DW, Shah K. TRAIL on trial: preclinical advances in cancer therapy. *Trends Mol Med*. 2013; 19: 685-94.
21. Mirandola P, Ponti C, Gobbi G, Sponzilli I, Vaccarezza M, Cocco L, et al. Activated human NK and CD8(+) T cells express both TNF-related apoptosis-inducing ligand (TRAIL) and TRAIL receptors but are resistant to TRAIL-mediated cytotoxicity. *Blood*. 2004; 104: 2418-24.
22. von Karstedt S, Montinaro A, Walczak H. Exploring the TRAILS less travelled: TRAIL in cancer biology and therapy. *Nat Rev Cancer*. 2017; 17: 352-66.
23. Jiang HH, Kim TH, Lee S, Chen X, Youn YS, Lee KC. PEGylated TNF-related apoptosis-inducing ligand (TRAIL) for effective tumor combination therapy. *Biomaterials*. 2011; 32: 8529-37.
24. Perlstein B, Finniss SA, Miller C, Okhrimenko H, Kazimirsky G, Cazacu S, et al. TRAIL conjugated to nanoparticles exhibits increased anti-tumor activities in glioma cells and glioma stem cells in vitro and in vivo. *Neuro Oncol*. 2013; 15: 29-40.
25. Kauer TM, Figueiredo JL, Hingtgen S, Shah K. Encapsulated therapeutic stem cells implanted in the tumor resection cavity induce cell death in gliomas. *Nat Neurosci*. 2011; 15: 197-04.
26. Park JS, Suryaprakash S, Lao YH, Leong KW. Engineering mesenchymal stem cells for regenerative medicine and drug delivery. *Methods*. 2015; 84: 3-16.
27. Santos JL, Pandita D, Rodrigues J, Pego AP, Granja PL, Tomas H. Non-viral gene delivery to mesenchymal stem cells: methods, strategies and application in bone tissue engineering and regeneration. *Curr Gene Ther*. 2011; 11: 46-57.
28. Riley MK, Vermerris W. Recent advances in nanomaterials for gene delivery-a review. *Nanomaterials*. 2017; 7: 94.
29. Wei QL, Chen Y, Ma XB, Ji JF, Qiao Y, Zhou B, et al. High-efficient clearable nanoparticles for multi-modal imaging and image-guided cancer therapy. *Adv Funct Mater*. 2018; 28: 1704634.
30. Liu Y, Yang Z, Huang X, Yu G, Wang S, Zhou Z, et al. Glutathione-responsive self-assembled magnetic gold nanowreath for enhanced tumor imaging and imaging-guided photothermal therapy. *ACS Nano*. 2018. 12: 8129-37.
31. Cheng XJ, Sun R, Yin L, Chai ZF, Shi HB, Gao MY. Light-triggered assembly of gold nanoparticles for photothermal therapy and photoacoustic imaging of tumors in vivo. *Adv Mater*. 2017; 29: 1604894.
32. Lu Y, Xu Y-J, Zhang G-b, Ling D, Wang M-q, Zhou Y, et al. Iron oxide nanoclusters for T1 magnetic resonance imaging of non-human primates. *Nat Biomed Eng* 2017; 1: 637-43.
33. Mekuria SL, Debele TA, Tsai HC. Encapsulation of gadolinium oxide nanoparticle (Gd<sub>2</sub>O<sub>3</sub>) contrasting agents in PAMAM dendrimer templates for enhanced magnetic resonance imaging in vivo. *ACS Appl Mater Interfaces*. 2017; 9: 6782-95.
34. Huang HY, Lovell JF. Advanced functional nanomaterials for theranostics. *Adv Funct Mater*. 2017; 27: 1603524.
35. Park JS, Yi SW, Kim HJ, Park KH. Receptor-mediated gene delivery into human mesenchymal stem cells using hyaluronic acid-shielded polyethylenimine/pDNA nanogels. *Carbohydr Polym*. 2016; 136: 791-02.
36. Zhu H, Mitsuhashi N, Klein A, Barsky LW, Weinberg K, Barr ML, et al. The role of the hyaluronan receptor CD44 in mesenchymal stem cell migration in the extracellular matrix. *Stem Cells*. 2006; 24: 928-35.
37. Huang RY, Chiang PH, Hsiao WC, Chuang CC, Chang CW. Redox-sensitive polymer/SPIO nanocomplexes for efficient magnetofection and MR imaging of human cancer cells. *Langmuir*. 2015; 31: 6523-31.
38. Xu YL, Qin Y, Palchoudhury S, Bao YP. Water-soluble iron oxide nanoparticles with high stability and selective surface functionality. *Langmuir*. 2011; 27: 8990-97.
39. Gupta AK, Gupta M. Cytotoxicity suppression and cellular uptake enhancement of surface modified magnetic nanoparticles. *Biomaterials*. 2005; 26: 1565-73.
40. Yang F, Cho SW, Son SM, Bogatyrev SR, Singh D, Green JJ, et al. Genetic engineering of human stem cells for enhanced angiogenesis using biodegradable polymeric nanoparticles. *Proc Natl Acad Sci U S A*. 2010; 107: 3317-22.
41. Lai PY, Huang RY, Lin SY, Lin YH, Chang CW. Biomimetic stem cell membrane-camouflaged iron oxide nanoparticles for theranostic applications. *Rsc Adv*. 2015; 5: 98222-30.
42. Schultz-Sikma EA, Joshi HM, Ma Q, Macrenaris KW, Eckermann AL, Dravid VP, et al. Probing the chemical stability of mixed ferrites: implications for MR contrast agent design. *Chem Mater*. 2011; 23: 2657-64.
43. Keunen O, Johansson M, Oudin A, Sanzey M, Rahim SAA, Fack F, et al. Anti-VEGF treatment reduces blood supply and increases tumor cell invasion in glioblastoma. *Proc Natl Acad Sci U S A*. 2011; 108: 3749-54.
44. Deng XJ, Zheng N, Song ZY, Yin LC, Cheng JJ. Trigger-responsive, fast-degradable poly(beta-amino ester)s for enhanced DNA unpacking and reduced toxicity. *Biomaterials*. 2014; 35: 5006-15.
45. Gabrielson NP, Pack DW. Efficient polyethylenimine-mediated gene delivery proceeds via a caveolar pathway in HeLa cells. *J Control Release*. 2009; 136: 54-61.
46. Pan SR, Cao DW, Fang R, Yi W, Huang H, Tian SQ, et al. Cellular uptake and transfection activity of DNA complexes based on poly(ethyleneglycol)-poly(L-glutamine) copolymer with PAMAM G2. *J Mater Chem B*. 2013; 1: 5114-27.
47. Iv M, Telischak N, Feng D, Holdsworth SJ, Yeom KW, Daldrup-Link HE. Clinical applications of iron oxide nanoparticles for magnetic resonance imaging of brain tumors. *Nanomedicine*. 2015; 10: 993-18.
48. Sasportas LS, Kasmieh R, Wakimoto H, Hingtgen S, van de Water JA, Mohapatra G, et al. Assessment of therapeutic efficacy and fate of engineered human mesenchymal stem cells for cancer therapy. *Proc Natl Acad Sci U S A*. 2009; 106: 4822-27.
49. Choi SA, Hwang SK, Wang KC, Cho BK, Phi JH, Lee JY, et al. Therapeutic efficacy and safety of TRAIL-producing human adipose tissue-derived mesenchymal stem cells against experimental brainstem glioma. *Neuro Oncol*. 2011; 13: 61-69.
50. Hervey-Jumper SL, Berger MS. Reoperation for recurrent high-grade glioma: a current perspective of the literature. *Neurosurgery*. 2014; 75: 491-99.
51. Kang MK, Kang SK. Tumorigenesis of chemotherapeutic drug-resistant cancer stem-like cells in brain glioma. *Stem Cells Dev*. 2007; 16: 837-47.
52. Sundahl N, Duprez F, Ost P, De Neve W, Mareel M. Effects of radiation on the metastatic process. *Mol Med*. 2018; 24: 16.
53. Yen SY, Chen SR, Hsieh J, Li YS, Chuang SE, Chuang HM, et al. Biodegradable interstitial release polymer loading a novel small

- molecule targeting Axl receptor tyrosine kinase and reducing brain tumour migration and invasion. *Oncogene*. 2016; 35: 2156-65.
54. Kidd S, Spaeth E, Dembinski JL, Dietrich M, Watson K, Klopp A, et al. Direct evidence of mesenchymal stem cell tropism for tumor and wounding microenvironments using in vivo bioluminescent imaging. *Stem Cells*. 2009; 27: 2614-23.
  55. Zheng B, von See MP, Yu E, Gunel B, Lu K, Vazin T, et al. Quantitative magnetic particle imaging monitors the transplantation, biodistribution, and clearance of stem cells in vivo. *Theranostics*. 2016; 6: 291-01.
  56. Kim SM, Woo JS, Jeong CH, Ryu CH, Lim JY, Jeun SS. Effective combination therapy for malignant glioma with TRAIL-secreting mesenchymal stem cells and lipoxygenase inhibitor MK886. *Cancer Res*. 2012; 72: 4807-17.
  57. Kim SM, Woo JS, Jeong CH, Ryu CH, Jang JD, Jeun SS. Potential application of temozolomide in mesenchymal stem cell-based TRAIL gene therapy against malignant glioma. *Stem Cells Transl Med*. 2014; 3: 172-82.